Flow Topology of Turbulent Natural and Forced Convection in a Vertical Channel Behind a Photovoltaic Panel: Numerical Study

Zineb OUAOUA [1*], *Kaoutar* KHALLAKI[1], *Khadija* CHOUKAIRY[1], and *Hafid* EL KHARAZ[1]

[1]Laboratory of Process, Energy, Materials and Environment Laboratory (PEME), National School of Applied Sciences of Khouribga, Sultan Moulay Slimane University, Beni-Mellal, Morocco.

Abstract. The performance of photovoltaic (PV) panels is greatly impacted by the efficiency with which heat is removed from their surface, especially in air-based cooling configurations. Although natural and forced convection in vertical air channels have been widely studied, the combined influence of channel depth and transitions in airflow regimes on PV cooling performance remains unclear. This study conducted a two-dimensional numerical analysis of the flow topology and thermal behavior of air circulation within an open vertical channel mounted behind a photovoltaic (PV) panel. Steady-state CFD simulations are performed using the standard k–ε turbulence model implemented in ANSYS Fluent. The effects of channel depth and airflow regimes, including natural, mixed, and forced convection, are investigated at a variety of inlet velocities. The results show that channel depth is an important factor in the development of flow and heat transfer. The optimal configuration is achieved by setting the channel depth to 10 mm and the inlet velocity to 2 m/s. This configuration has been shown to reduce the PV panel temperature by over 10.7% compared to pure natural convection alone. This thermal enhancement demonstrates the potential of optimised air channels to minimise temperature-induced efficiency losses in photovoltaic modules.

Nomenclature

H	length of channel (m)	Ri	Richardson number
b	depth of channel (m)	Nu	Nusselt number $Nu = \frac{hb}{\lambda}$
x_i	cartesian coordinates (x, y)	$Nu_{1/2}$	average Nusselt number at mid-height
q	heat flux (W/m^2)	Ra^*	modified Rayleigh number
g	gravitational acceleration $g = 9.81 m/s^2$	Pr	Prandtl number $Pr = \frac{\mu C_p}{\lambda}$
p	pressure (Pa)	LB	Local Bernoulli

* Corresponding author: zineb.ouaoua@usms.ac.ma

U_i	average velocity coordinates (m/s)	**Greek symbols**	
C_p	specific heat (J/Kg.K)		
v	the velocity in y direction (m/s)	ρ_0	constant density (Kg/m^3)
k	turbulent kinetic energy (m^2/s^2)	C_ε	empirical constant
σ_t	Nombre Prandtl turbulent	μ_t	turbulent dynamic viscosity
σ_k	Nombre Prandtl turbulent de k	ν	kinematic viscosity
σ_ϵ	Nombre Prandtl turbulent de ϵ	ν_t	turbulent kinematic viscosity
Vin	velocity at inlet (m/s)	σ_t	turbulent Prandtl number
T	Temperature (K)	λ	thermal conductivity of fluid (w/m.k)
T_{amb}	ambient temperature	ε	the specific rate of dissipation
h	local heat transfer coefficient		
LB-0	P=0 at the outlet $p = -0.5v^2$ at the inlet		
LB-LB	$p = -0.5v^2$ at the outlet $p = -0.5v^2$ at the inlet		
G_k	production of turbulent kinetic energy due to buoyancy		
P_k	production of turbulent kinetic energy due to velocity		

1 Introduction

Photovoltaic (PV) technology has been widely adopted as a renewable energy source due to its sustainable performance, flexible deployment, and minimal environmental impact [1]. However, the electrical efficiency of PV modules remains strongly dependent on their operating temperature [2,3]. Typically, only 15–22% of the incident solar radiation is converted into electrical energy under outdoor conditions, with the remaining fraction dissipating as heat within the PV structure [4]. This heat accumulation leads to a significant rise in module temperature, which negatively affecting electrical efficiency and accelerating material degradation. Consequently, effective thermal management has become a critical aspect of the design and operation of photovoltaic installations [5,6].

Various strategies have been proposed to reduce PV overheating. Air-based cooling methods have attracted considerable attention due to their ease of implementation, affordability and compatibility with PV systems. In particular, open vertical air channels installed behind PV panels provide a passive or semi-passive cooling solution, in which buoyancy-induced airflow helps to carry heat away from the rear of the module. Natural convection is an environmentally friendly solution that requires no additional energy input in such configurations. However, its cooling capacity is often limited, particularly in conditions of high solar irradiance and low ambient wind speed [7]. Consequently, several authors have

demonstrated that natural convection alone is frequently insufficient to maintain PV modules within their optimal operating temperature range. In order to address this shortcoming, many studies have investigated the potential of forced convection, which involves introducing an external airflow through the cooling channel. The results generally suggest that increasing the airflow rate improves heat transfer and can lead to measurable improvements in the electrical performance of PV systems. Ibrahim et al. [8] conducted an experimental parametric study comparing free and forced convection conditions. They reported an efficiency increase of around 11%, as well as economic advantages and reduced CO_2 emissions. Overall, these results highlight the potential of airflow-assisted cooling for photovoltaic applications. That said, using forced convection makes the system more complex and increases energy consumption. Therefore, it is necessary to strike a balance between cooling performance and design simplicity.

In addition to the airflow rate, the geometric characteristics of the cooling channel are crucial in determining the system's thermal and hydrodynamic behaviour. In particular, channel depth directly influences the development of the boundary layer, the stability of the flow and the mechanisms of heat transfer.[9] Several studies based on numerical simulations and experiments have focused on natural and mixed convection in vertical channels. These studies usually consider uniform heat flux or constant wall temperature conditions. Chen et al. [9] demonstrated that lower aspect ratios and enhanced secondary circulation can significantly improve thermal performance in mixed convection regimes. Other studies have reported that reverse flow and recirculation zones may occur in wider channels. This phenomenon can potentially compromise convective heat transfer, despite an increase in channel dimensions.

Despite the growing body of literature on PV cooling and convective heat transfer in vertical channels, significant gaps remain. Most existing studies focus on either purely natural or fully forced convection, while the transition between these regimes is often simplified. Furthermore, the combined effect of channel depth and transition between airflow regimes (natural, mixed and forced convection) on the cooling performance of PV-mounted air channels has not yet been systematically analysed. Design-oriented studies that identify optimal channel dimensions under different operating regimes are particularly limited.

This study aims to overcome these limitations by conducting a thorough numerical analysis of airflow and heat transfer in an open vertical air channel positioned behind a photovoltaic panel. A two-dimensional computational fluid dynamics (CFD) model was created using ANSYS Fluent to examine the interaction between channel depth and inlet velocity across a wide range of operating conditions. The Richardson number criterion is used to clearly identify the natural, mixed and forced convection regimes, allowing a comprehensive analysis of the regime transitions. Temperature fields, velocity distributions, streamlines and Nusselt numbers are examined in order to characterise the flow topology and thermal performance.

This work makes three key contributions. Firstly, it provides a comprehensive physical understanding of the flow structures and heat transfer behaviour that occur with varying channel depths. Secondly, it clarifies the impact of a transition in the airflow regime on PV cooling efficiency. Finally, it identifies the optimal channel configurations for natural, mixed and forced convection conditions, offering practical guidelines for the design of compact and efficient air-cooled photovoltaic systems.

2 Physical model description

2.1 Numerical proceeding

Turbulent flow in the vertical channel was simulated using a Computational Fluid Dynamics (CFD) solver. The governing equations were discretized using the finite volume method (FVM), and pressure–velocity coupling was achieved through the coupled algorithm, which ensures stable convergence in the case of buoyancy-driven flows involving strong thermo-fluid interactions. To enhance numerical accuracy, the momentum, energy, turbulent kinetic energy (k) and turbulence dissipation rate (ε) equations were discretized using a second-order upwind scheme. Convergence was assumed when the residuals for continuity and momentum fell below 10^{-5}. A stricter criterion of 10^{-7} was, however, imposed for the energy equation, in order to ensure accurate thermal predictions. Enhanced wall functions were applied to resolve near-wall flow behavior appropriately, while maintaining computational efficiency.

2.2 Geometrical model and assumptions

The physical model comprises an opening vertical air channel formed by two parallel plates that represent the air gap between a photovoltaic panel and its support. The channel height is fixed at 640 mm, which is typical for a PV module. Its depth varies from 10 to 90 mm in order to study the effect on flow and heat transfer. The rear surface of the PV is heated with a uniform heat flux, while the opposite wall is adiabatic. Allowing airflow to develop naturally through open inlet and outlet boundaries, the channel depth has a strong influence on boundary layer growth, buoyancy effects, flow stability and recirculation. A 2D representation is adopted based on Dupont [10] who showed that side-wall effects are negligible, capturing the main thermal and flow behaviors accurately.

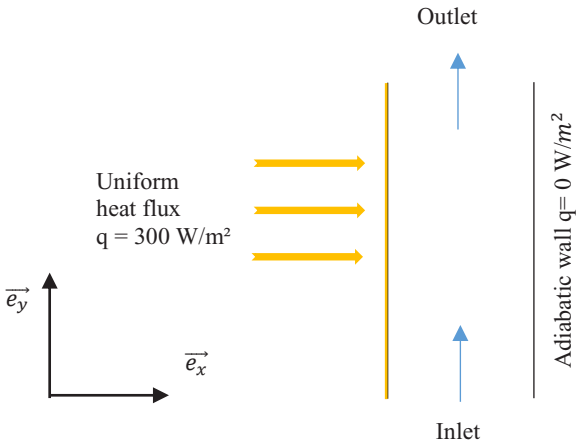

Fig. 1. Geometrical model of an air channel.

2.3 Mathematical model

The two-dimensional governing equations for continuity, momentum, and energy are solved using the Boussinesq approximation, assuming steady, incompressible, Newtonian flow. Air properties are constant, and turbulence is modeled with the standard k–ε approach [12].

Continuity equation:

$$\frac{\partial u}{\partial x}+\frac{\partial v}{\partial y}=0 \quad (1)$$

Momentum equations:

$$\frac{\partial(\rho_0 u_j u_{i_i})}{\partial x_j}=-\frac{\partial P}{\partial x_i}+\frac{\partial}{\partial x_j}\left[(\mu+\mu_t)\left(\frac{\partial u_i}{\partial x}+\frac{\partial u_j}{\partial x}-\frac{2}{3}\frac{\partial u_k}{\partial x_k}\right)\delta_{ij}\right]+\rho g_i \quad (2)$$

Energy equation:

$$\frac{\partial(\rho u_j C_p T)}{\partial x_j}=\frac{\partial\left[\left(\lambda+\frac{\mu_t c_p}{\sigma_t}\right)\frac{\partial T}{\partial x_j}\right]}{\partial x_j}+\frac{\partial u_i}{\partial x_j}\left[(\mu+\mu_t)\left(\frac{\partial u_i}{\partial x_j}+\frac{\partial u_j}{\partial x_i}-\frac{2}{3}\frac{\partial u_k}{\partial x_k}\right)\delta_{ij}\right]+u_j\frac{\partial p}{\partial x_j} \quad (3)$$

Standard k-ε Turbulence Model Equations [11]:

Turbulent Kinetic Energy (k):

$$\rho\left(u\frac{\partial k}{\partial x}+v\frac{\partial k}{\partial y}\right)=\frac{\partial}{\partial x}\left(\left(\mu+\frac{\mu_t}{\sigma_k}\right)\frac{\partial k}{\partial x}\right)+\frac{\partial}{\partial y}\left(\left(\mu+\frac{\mu_t}{\sigma_k}\right)\frac{\partial k}{\partial y}\right)+P_k+G_k-\rho\epsilon \quad (4)$$

Dissipation Rate (ε):

$$\rho\left(u\frac{\partial \epsilon}{\partial x}+v\frac{\partial \epsilon}{\partial y}\right)=\frac{\partial}{\partial x}\left(\left(\mu+\frac{\mu_t}{\sigma_\epsilon}\right)\frac{\partial \epsilon}{\partial x}\right)+\frac{\partial}{\partial y}\left(\left(\mu+\frac{\mu_t}{\sigma_\epsilon}\right)\frac{\partial \epsilon}{\partial y}\right)+C_{1\epsilon}\frac{\epsilon}{k}(P_k+C_{3\epsilon}G_k)-C_{2\epsilon}\rho\frac{\epsilon^2}{k} \quad (5)$$

Where: u_j and u_i are the velocity components, p is the pressure, ρ is the fluid density, μ is the dynamic viscosity, T is the temperature, C_p is the specific heat capacity, λ is the thermal conductivity, σ_k and σ_ε are the turbulent Prandtl numbers, P_k is the production of turbulent kinetic energy due to velocity gradients, $G_k$is the production of turbulent kinetic energy due to buoyancy, and $C_{1\varepsilon}$, $C_{2\varepsilon}$, and $C_{3\varepsilon}$ are empirical constants. [11]

2.4 Boundary conditions

This numerical study considers an open vertical channel to enable continuous fluid recirculation between the cooling channel's inlet and outlet. Proper boundary conditions are essential for accurately resolving the coupled thermo-hydrodynamic processes.

The heated wall is subjected to a uniform heat flux of 300 W/m², while the opposite wall is adiabatic. For forced convection, a velocity inlet is imposed with speeds ranging from 0,5 to 2m/s. For natural convection, a pressure inlet is applied at the inlet, along with a local Bernoulli condition LB-0 which produces a more pronounced reverse flow than LB-LB. According to [12], local Bernoulli conditions LB-0 have been chosen here for the channel inlet and outlet, and ambient temperature is set to T_{amb}=298K. The pressure at the outlet is equal to atmospheric pressure.

3 Numerical model

3.1 Mesh validation

A grid independence study was performed to ensure numerical accuracy while minimizing computational cost. Several structured meshes were tested, and a final mesh of 102,400 cells

was selected for all simulations. The mesh was refined near the heated wall to accurately capture the thermal and velocity boundary layers. Increasing mesh density beyond this value resulted in negligible changes in the mean Nusselt number and skin friction coefficient (< 0.5%), confirming the adequacy of the chosen mesh resolution. This approach guarantees a reliable balance between computational efficiency and numerical precision.

3.2 Validation model

The numerical model was validated using experimental data on natural convection in vertical air channels from Webb & Hill [13]. The comparison showed good agreement, particularly for modified Rayleigh numbers Ra^* above 1.5×10^4, with a maximum deviation of 7.1% at lower Rayleigh numbers.
The present study produced the following mid-height local Nusselt number correlation:

$$\mathrm{Nu} = 0{,}734 Ra^{*0{,}189}$$

while Webb's experimental correlation is given by:

$$\mathrm{Nu} = 0{,}58 Ra^{*0{,}206}$$

Fig. 2 shows a comparison between the present numerical results and the experimental data reported by Webb & Hill [13]. The results are in good agreement over the studied range of modified Rayleigh numbers, which supports the validity of the numerical model for predicting heat transfer in vertical air channels.

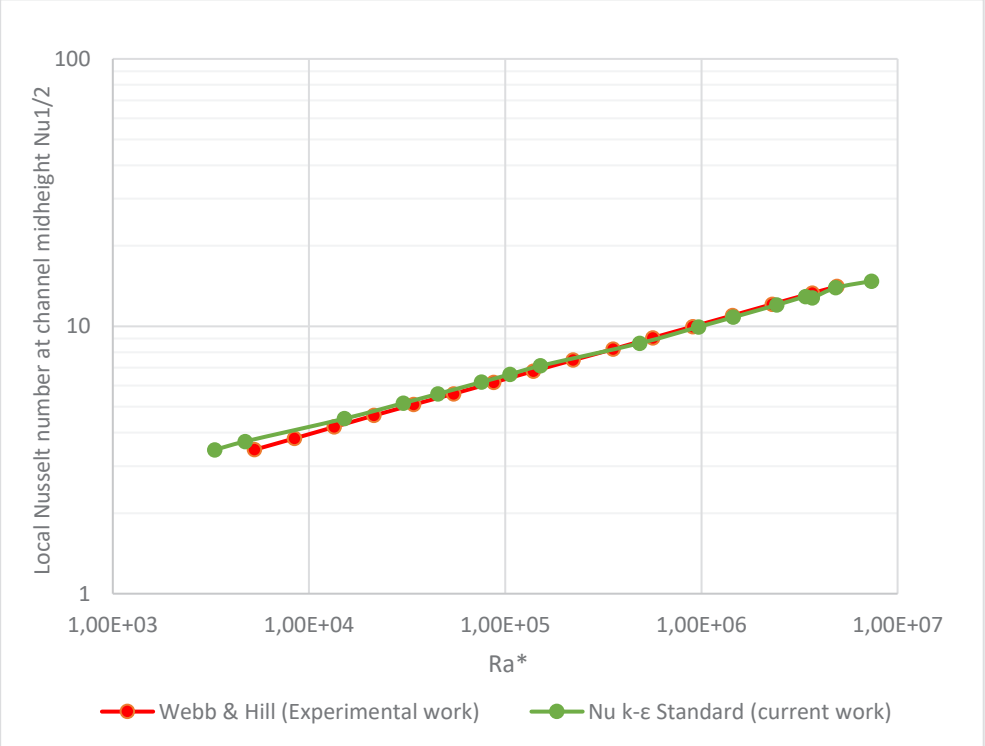

Fig. 2. Comparison between the present numerical results and Webb's experimental data for the variation of the local Nusselt number with the modified Rayleigh number.

This validation shows that the numerical approach can accurately predict the heat transfer characteristics of vertical channels under natural convection. The slight differences observed at lower Ra* values are due to the limitations of the experimental measurements and the two-dimensional approximation adopted in this study. Overall, the model reliably frames the study of the combined impact of channel depth and inlet velocity on the natural, mixed and forced convection regimes behind PV panels.

4 Results and Discussion

A comprehensive analysis was carried out to investigate how channel depth and inlet velocity influence the thermal and flow behavior within the air-cooling channel. The performance is evaluated using wall temperature distributions, streamlines, velocity contours and average Nusselt numbers. These factors provide a comprehensive overview of the dominant heat-transfer mechanisms.

4.1 Channel depth effect on thermal and flow behavior for natural convection

This section focuses on the impact of channel depth on the structure of the flow and the performance of heat transfer under natural convection conditions. The corresponding streamlines and temperature contours for various channel depths are presented in Fig. 3.

Streamlines		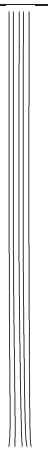			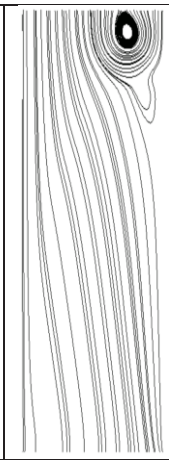
Depth(mm)	10	15	30	60	90

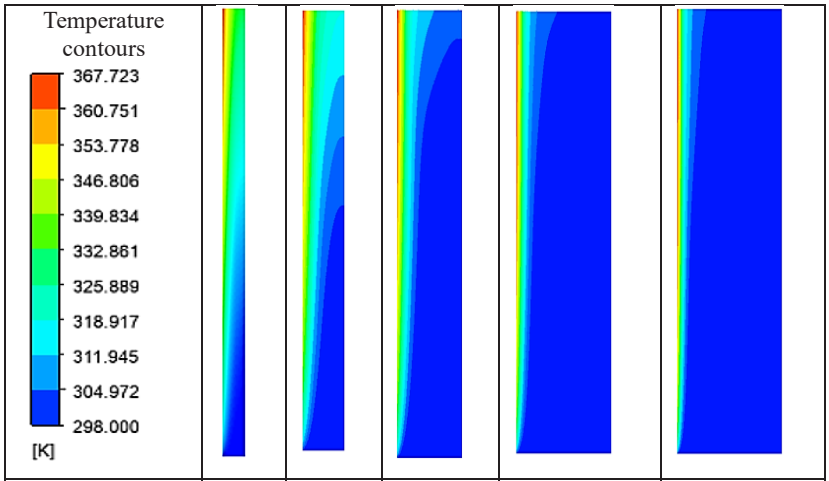

Fig. 3. (a) streamlines (b) temperature contours for different channel depths.

The results show that channel depth has a significant impact on the flow structure, thermal boundary layer development, and overall heat transfer performance (Fig. 3a).
For depths of 30 mm or less, the flow becomes progressively more organised and fully developed along the channel. The formation of stable boundary layers near the walls promotes predictable, buoyancy-driven motion and enhances convective heat transfer. However, for a channel that is very narrow (b = 10 mm), there is insufficient space for the thermal boundary layer to develop fully. As shown in Fig. 3a, buoyancy-induced motion is weak and heat transfer is dominated by conduction. This results in poor cooling performance.

The flow structure changes markedly when the channel depth exceeds 30 mm. A well-defined boundary layer forms near the heated wall, and a recirculation zone develops close to the adiabatic wall near the outlet. This reverse flow is driven by buoyancy forces and constraints on mass conservation, producing a characteristic V-shaped flow pattern. In this pattern, cooler air enters through the outlet and descends along the adiabatic wall. This recirculation reduces the upward velocity of the main flow, weakening convective transport and deteriorating cooling effectiveness.

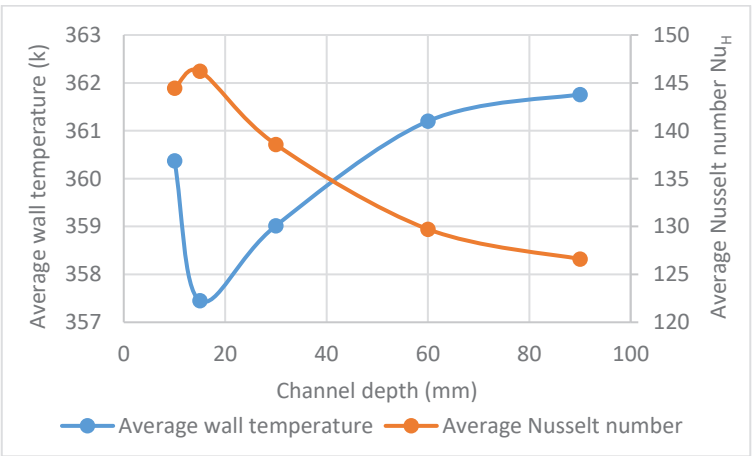

Fig. 4. Average wall temperature and average Nusselt number for different channel depths.

The temperature contours presented in Fig. 3b illustrate how channel depth affects heat transfer. For b ≥ 30 mm, the high-temperature region is confined to a thin thermal boundary layer next to the heated wall, while the rest of the channel remains relatively cool. Increasing the channel depth beyond this value does not improve convective heat transfer. Instead, intensified reverse flow recirculation restricts the entrainment of cold air and leads to a degradation of thermal performance. This trend is confirmed by the quantitative results shown in Fig. 4, which demonstrate that an increase in channel depth beyond 30 mm leads to a higher average wall temperature and a lower average Nusselt number.
A detailed analysis of Fig. 4 indicates that the optimal channel depth occurs at b = 15 mm, where thermal performance is maximized. At this depth, the wall temperature decreases to its minimum value of 356 K, while the average Nusselt number attains a maximum value above 362. This demonstrates that the thermal boundary layer and buoyancy-driven flow are most efficiently developed at b = 15 mm, with no recirculation zones present. Therefore, b = 15 mm represents the optimal channel depth for natural convection in the present study.

This analysis shows that channel depth is crucial in determining the development of buoyancy-driven flow and the resulting heat transfer performance. However, the geometry of the channel alone is insufficient to control the system's thermal behaviour. In practical applications, introducing an imposed airflow significantly alters the flow structure and heat-transfer mechanisms. The following section therefore examines the effect of inlet velocity on the transition between the natural, mixed, and forced convection regimes.

4.2 Effect of inlet velocity on flow structure and heat-transfer performance

This section examines how inlet velocity affects the structure of the airflow and heat transfer. The evolution of the velocity profiles inside the channel and their effect on heat transfer are shown in Fig. 5. The aim of the analysis is to clarify how the imposed airflow modifies the dominant heat-transfer mechanisms and the transition between different convection regimes.

Streamlines	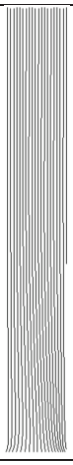		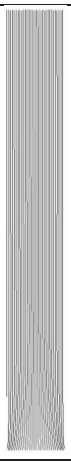	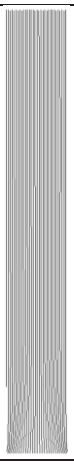	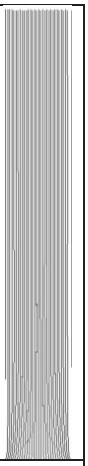
Velocity (m/s)	Natural convection	Vin=0,5	Vin=1	Vin=1,5	Vin=2

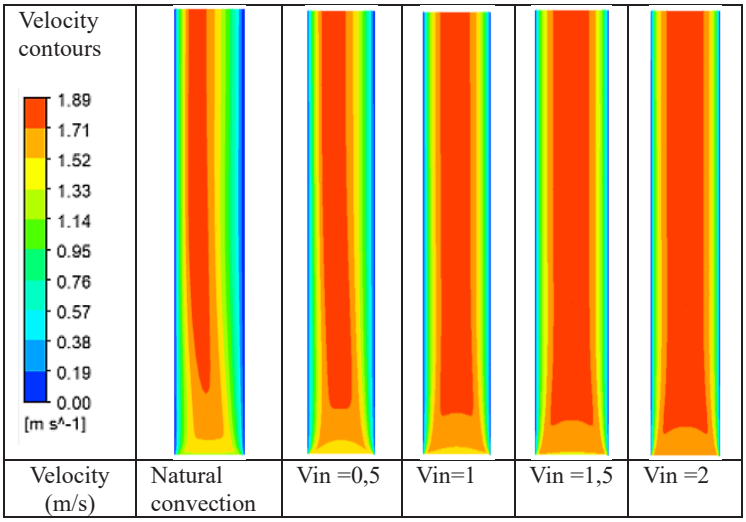

Fig. 5: (a) streamlines (b) velocity contours for different inlet velocity.

In the natural convection regime (Ri > 10), the flow is insufficiently developed and velocities remain low, which limits its ability to remove heat. Consequently, the Nusselt number is low. Under these conditions, buoyancy forces alone are insufficient to generate vigorous upward flow, resulting in weak convective heat transfer.

For an inlet velocity of 0.5 m/s, the corresponding Richardson number is $0.1 < Ri < 10$ [14], which is in the mixed convection regime. In this intermediate regime, both buoyancy and inertial forces contribute to the flow development. In this configuration, the flow becomes more organised and developed along the channel. This results in better internal mixing and improved momentum transport towards the heated wall. The reorganised flow structure is clearly visible in the streamlines and velocity contours shown in Fig. 5. This results in a significant increase in the Nusselt number, which indicates an improvement in heat transfer caused by the combined effects of buoyancy and forced flow. At imposed velocities greater than 1 m/s ($Vin \geq 1$ m/s), the Richardson number becomes less than 0.1 ($Ri < 0.1$) [15], indicating that the flow is fully dominated by forced convection.

The imposed inertia suppresses buoyancy-induced instabilities, promoting a uniform, high-velocity flow upwards. In this regime, the Nusselt number reaches its maximum value, indicating the flow's significantly enhanced ability to remove heat from the heated wall.

Fig. 6 shows that as the inlet velocity increases, the flow progressively transitions from natural convection to mixed convection, and eventually to forced convection. The imposed airflow significantly enhances the fluid velocity inside the channel, strengthening momentum transport and thermal mixing near the heated wall. Consequently, the average Nusselt number increases continuously, indicating an improvement in convective heat transfer intensity, while the average wall temperature decreases. In contrast, under natural convection, the flow velocity remains weak and negligible compared to forced convection, leading to limited heat transfer and higher wall temperatures.

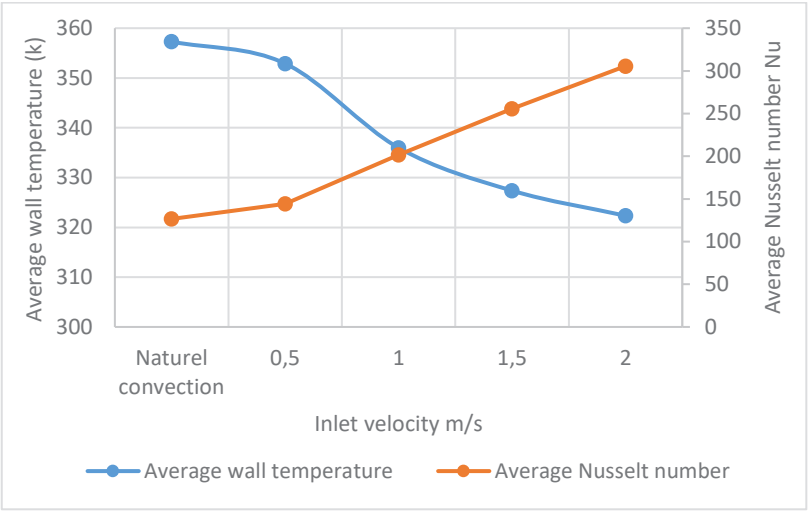

Fig. 6. Average wall temperature and average Nusselt number for different inlet velocity.

Fig. 7 shows that the wall temperature depends on the air velocity and channel depth. Increasing the inlet velocity enhances forced convection, reducing the wall temperature. In contrast, a larger channel depth weakens flow development, leading to a higher hot-wall temperature. This trend highlights the strong coupling between channel geometry and the intensity of the imposed airflow.

For natural convection, a depth of b = 15 mm is optimal. By contrast, a depth of b =10 mm is most effective for mixed and forced convection. In narrow channels with an imposed inlet velocity, flow confinement plays a key role in the system's thermal behavior. It increases the local air speed, promoting a more organized flow structure and strengthening forced convection to enhance wall cooling. Consequently, optimising both the inlet velocity and the channel depth significantly reduces the PV operating temperature.

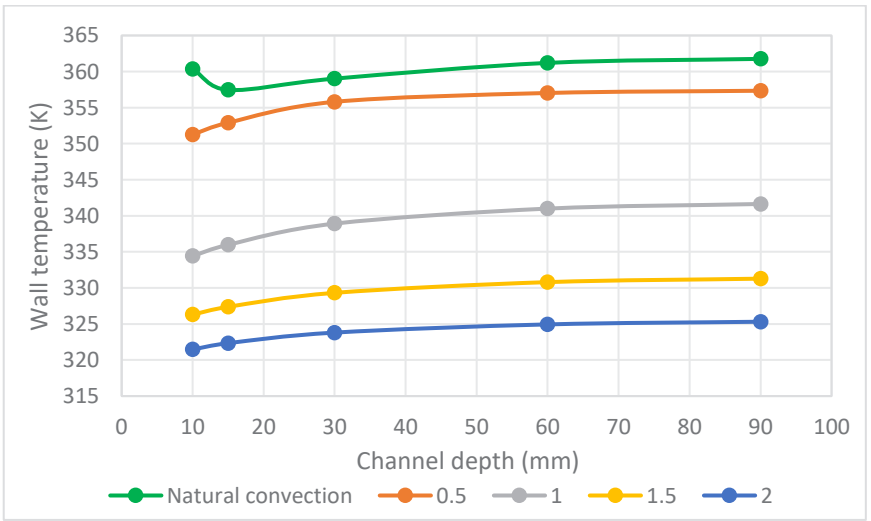

Fig. 7. Average Wall temperature of heated wall for different channel depths and inlet velocity

Conclusion

This study investigated the thermal and flow behavior of air circulation within an open vertical channel positioned behind a photovoltaic panel, considering the effects of natural, mixed and forced convection. A two-dimensional numerical approach was used to analyze the combined impact of channel depth and inlet velocity on heat transfer performance.

The results show that channel depth is crucial in determining the development of buoyancy-driven flow and the related heat transfer mechanisms. When natural convection is the dominant factor, the most optimal configuration is achieved with a channel depth of b = 15 mm. At this depth, the thermal boundary layer develops completely without causing flow recirculation. This results in lower wall temperatures and higher average Nusselt numbers.

For mixed and forced convection regimes, the optimal configuration is a narrow channel with a depth of b = 10 mm. In this case, the combination of flow confinement and an imposed inlet velocity enhances local air speed, suppresses buoyancy-induced recirculation and strengthens forced convection. Consequently, the wall temperature decreases significantly, with a maximum reduction of over 10.7% compared to natural convection. The influence of inlet velocity was also found to be significant. Increasing the inlet velocity clearly causes a transition in the flow from being buoyancy-dominated ($Ri > 10$) to mixed convection ($0.1 < Ri < 10$) and finally to forced convection ($Ri < 0.1$). This transition is characterised by progressive flow structuring, enhanced momentum transport towards the heated wall and a significant rise in the Nusselt number.

Overall, the results highlight the strong coupling between channel geometry and operating airflow conditions. To be efficient cooling design cannot rely solely on natural convection or geometric optimization, they must also account for the interaction between confinement effects and imposed airflow.

From a practical perspective, the findings offer clear design guidelines for compact, efficient photovoltaic cooling systems. Selecting an appropriate channel depth and inlet velocity can significantly reduce the operating temperature of PV systems, improve electrical efficiency and mitigate temperature-induced performance degradation.

References

[1] E. Skoplaki, J.A. Palyvos, On the temperature dependence of photovoltaic module electrical performance: A review of efficiency/power correlations, Sol. Energy 83 (2009) 614–624. https://doi.org/10.1016/j.solener.2008.10.008.

[2] H. El Kharaz, K. Khallaki, M.S. Kadiri, K. Choukairy, A numerical analysis of air flow topology within a vertical channel attached behind photovoltaic panel, Int. J. Heat Mass Transf. 223 (2024) 125254. https://doi.org/10.1016/j.ijheatmasstransfer.2024.125254.

[3] G. Gan, Simulation of buoyancy-driven natural ventilation of buildings—Impact of computational domain, Energy Build. 42 (2010) 1290–1300. https://doi.org/10.1016/j.enbuild.2010.02.022.

[4] G. Gan, Effect of air gap on the performance of building-integrated photovoltaics, Energy 34 (2009) 913–921. https://doi.org/10.1016/j.energy.2009.04.003.

[5] A.S. Fahad M, K. Osman, U. Abidin, M.S. Ahmad, E.M. Housein Ismaeil, M.U. Farooq, Review of Cooling Techniques for Improving Solar Photovoltaic Panel Efficiency, J. Adv. Res. Fluid Mech. Therm. Sci. 125 (2024) 193–219. https://doi.org/10.37934/arfmts.125.1.193219.

[6] M. Farshchimonfared, J.I. Bilbao, A.B. Sproul, Channel depth, air mass flow rate and air distribution duct diameter optimization of photovoltaic thermal (PV/T) air collectors linked to residential buildings, Renew. Energy 76 (2015) 27–35. https://doi.org/10.1016/j.renene.2014.10.044.

[7] O. Zogou, H. Stapountzis, Experimental validation of an improved concept of building integrated photovoltaic panels, Renew. Energy 36 (2011) 3488–3498. https://doi.org/10.1016/j.renene.2011.05.034.

[8] T. Ibrahim, J. Faraj, K. Kisswani, G.E. Achkar, R. Murr, M. Khaled, Cooling photovoltaic panels with air convection – Parametric environmental and economic analysis with case studies, E-Prime - Adv. Electr. Eng. Electron. Energy 12 (2025) 101020. https://doi.org/10.1016/j.prime.2025.101020.

[9] Q. Chen, N. Harris, K.J. Craig, M. Everts, Mixed convective laminar flow through non-circular channels heated at a constant heat flux, Int. J. Therm. Sci. 210 (2025) 109664. https://doi.org/10.1016/j.ijthermalsci.2024.109664.

[10] D. Frédéric, T. Fabien, S. Sandrine, B. Ruddy, Two-dimension experimental study of the reverse flow in a free convection channel with active walls differentially heated, Exp. Therm. Fluid Sci. 47 (2013) 150–157. https://doi.org/10.1016/j.expthermflusci.2013.01.010.

[11] T. Yilmaz, S.M. Fraser, Turbulent natural convection in a vertical parallel-plate channel with asymmetric heating, Int. J. Heat Mass Transf. 50 (2007) 2612–2623. https://doi.org/10.1016/j.ijheatmasstransfer.2006.11.027.

[12] B. Brangeon, P. Joubert, A. Bastide, Influence of the dynamic boundary conditions on natural convection in an asymmetrically heated channel, Int. J. Therm. Sci. 95 (2015) 64–72. https://doi.org/10.1016/j.ijthermalsci.2015.04.006.

[13] B.W. Webb, D.P. Hill, High Rayleigh Number Laminar Natural Convection in an Asymmetrically Heated Vertical Channel, J. Heat Transf. 111 (1989) 649–656. https://doi.org/10.1115/1.3250732.

[14] C Tian, J Wang, Experimental study on mixed convection in an asymmetrically heated, inclined, narrow, rectangular channel, Int. J. Heat Mass Transf. 116 (2018) 1074–1084. https://doi.org/10.1016/j.ijheatmasstransfer.2017.09.099.

[15] A.K. Azad, A. Abid, C.N. Mithun, Md.J. Hasan, R. Hossain, M.M. Rahman, Effect of Richardson number on transient double diffusive mixed convection: A thermo-hydrodynamic study, Int. J. Thermofluids 17 (2023) 100273. https://doi.org/10.1016/j.ijft.2022.100273.